Electronic Supplementary Material (ESI) for Journal of Materials Chemistry A.
This journal is © The Royal Society of Chemistry 2023

Supplementary Information

Metal-Free Covalent Organic Frameworks Containing Precise Heteroatoms for Electrocatalytic Oxygen Reduction Reaction

Jiali Li, Ji Jia, Jinquan Suo, Cuiyan Li, Zhiwei Wang, Hui Li,* Valentin Valtchev, Shilun Qiu, Xiaoming Liu,* and Qianrong Fang*

Table of Contents

1. Experimental Procedures

1.1 Materials

All starting materials and solvents, unless otherwise noted, were obtained from J&K Scientific LTD. Benzotrithiophene tricarbaldehyde (BTT) was purchased from Jilin Extension Technology. Mesitylene and 1,4-dioxane were obtained from J&K Scientific LTD.

1.2 Synthesis and Characterization

Synthesis of 4,4'-(Benzoselenadiazole-4,7-diyl) diaminobenzene (BSD)

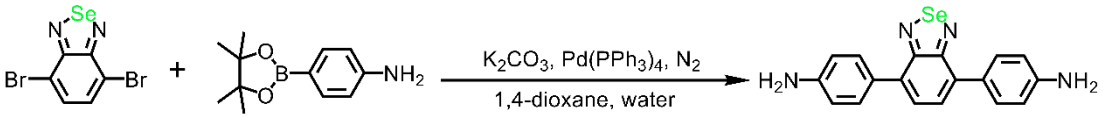

4,7-dibromo-2,1,3-benzoselenadiazole (1.6 g, 4.69 mmol), 4-aminophenylboronic acid pinacol ester (2.26 g, 10.32 mmol), K_2CO_3 (1.94 g, 10.07 mmol) and $Pd(PPh_3)_4$ (54.52 mg, 0.47 mmol) were added into the mixture solution of 1,4-dioxane (45 mL) and water (15 mL). The mixture was degassed for 30 min and then refluxed under N_2 atmosphere for 3 days. After cooling down to room temperature, the formed precipitate was poured into water and extracted by dichloromethane for three times. After the solvent was evaporated, the crude product was chromatographed on silica gel using DCM/PE=4/1 as an eluent to afford a red solid. Yield: 1.2 g (68%). ^{1}H NMR (400MHz, $CHCl_3$): δ 7.76 (d, 4H), δ 7.56 (s, 2H), δ 6.87 (d, 4H), δ 3.86 (s, 4H). FT-IR (KBr, cm^{-1}): 3400, 3335, 1610, 1514, 1463, 1358, 1279, 1187, 829, 647, 530.

Synthesis of 4,4'-(Benzothiadiazole-4,7-diyl) diaminobenzene (BTD)

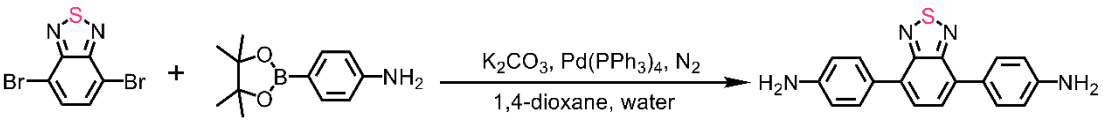

Similar to the synthesis of BSD, 4,7-dibromo-2,1,3-benzothiadiazole (1.4 g, 4.69 mmol), 4-aminophenylboronic acid pinacol ester (2.26 g, 10.32 mmol), K_2CO_3 (1.94 g, 10.07 mmol) and $Pd(PPh_3)_4$ (54.52 mg, 0.47 mmol) were added into the mixture solution of 1,4-dioxane (45 mL) and water (15 mL). The mixture was degassed for 30 min and then refluxed under N_2 atmosphere for 3 days. After cooling down to room temperature, the formed precipitate was poured into water and extracted by dichloromethane for three times. After the solvent was evaporated, the crude product was chromatographed on silica gel using DCM/PE = 4/1 as an eluent to

afford an orangered solid.[1] Yield: 926 mg (62%). ^{1}H NMR (400MHz, $CHCl_3$): δ 7.86 (d, 4H), δ 7.72 (s, 2H), δ 6.89 (d, 4H), δ 3.88 (s, 4H). FT-IR (KBr, cm^{-1}): 3471, 3371, 1620, 1518, 1478, 1347, 1282, 1370, 1190, 822, 601, 534.

Synthesis of 4,4'-(Benzoxadiazole-4,7-diyl) diaminobenzene (BXD)

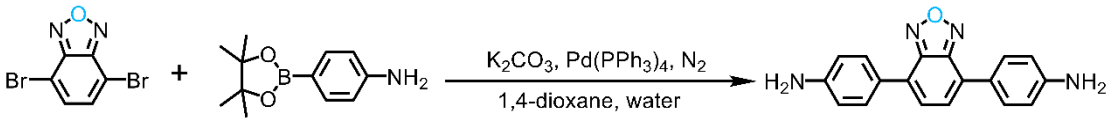

Similar to the synthesis BSD and BTD, 4,7-dibromo-2,1,3-benzoxadiazole (1.3 g, 4.69 mmol), 4-aminophenylboronic acid pinacol ester (2.26 g, 10.32 mmol), K_2CO_3 (1.94 g, 14.07 mmol) and Pd $(PPh_3)_4$ (54.52 mg, 0.47 mmol) were added into the mixture solution of 1,4-dioxane (45 mL) and water (15 mL). The mixture was degassed for 30 min and then refluxed under N_2 atmosphere for 3 days. After cooling down to room temperature, the formed precipitate was poured into water and extracted by dichloromethane for three times. After the solvent was evaporated, the crude product was chromatographed on silica gel using dichloromethane/petroleum ether = 4/1 (DCM/PE = 4/1) as an eluent to afford a dark red solid. Yield: 922 mg (65%). ^{1}H NMR (400MHz, $CHCl_3$): δ 7.93 (d, 4H), δ 7.57 (s, 2H), δ 6.86 (d, 4H), δ 3.93 (s, 4H). FT-IR (KBr, cm^{-1}): 3483, 3387, 1613, 1511, 1436, 1383, 1291, 1186, 828, 603, 537.

Synthesis of JUC-616

BTT (0.04 mmol, 13 mg) and BSD (0.06 mmol, 22.0 mg) were weighted into a Pyrex tube (volume: ca. 20.0 mL with a body length of 18.0 cm, neck length of 9 cm) and to the mixture was added mesitylene (0.6 mL), 1,4-dioxane (0.4 mL) and 0.1 mL of aqueous acetic acid (6.0 mol/L). The Pyrex tube was flash frozen in a liquid nitrogen bath, evacuated to an internal pressure of ca. 19.0 mbar and flame-sealed, reducing the total length by ca. 10.0 cm. Upon warming to room temperature, the tube was placed in an oven at 120 °C for four days. As a result, a brown powder was isolated by centrifugation and washed with acetone (3 × 5.0 mL) and the yield is about 90%. Anal. Cald: C: 61.09; H: 2.54; N: 10.18; S: 11.64; Se: 14.55. Found: C: 61.65; H: 2.24; N: 10.02; S: 11.86; Se: 14.23.

Synthesis of JUC-617

Similar to the synthesis of JUC-616, BTT (0.04 mmol, 13 mg) and BTD (0.06 mmol, 19.0 mg) were weighted into a Pyrex tube (volume: ca. 20.0 mL with a body length of 18.0 cm, neck length of 9 cm) and to the mixture

was added mesitylene (0.5 mL), 1,4-dioxane (0.5 mL) and 0.1 mL of aqueous acetic acid (6.0 mol/L). The Pyrex tube was flash frozen in a liquid nitrogen bath, evacuated to an internal pressure of ca. 19.0 mbar and flame-sealed, reducing the total length by ca. 10.0 cm. Upon warming to room temperature, the tube was placed in an oven at 120 °C for three days. As a result, a red powder was isolated by centrifugation and washed with acetone (3 × 5.0 mL), and the yield is about 87%. Anal. Cald: C: 66.93; H: 2.79; N: 11.16; S: 19.12. Found: C: 67.11; H: 2.03; N: 10.98; S: 19.88.

Synthesis of JUC-618

Similar to the synthesis of JUC-616 and JUC-617, BTT (0.04 mmol, 13 mg) and BXD (0.06 mmol, 18.0 mg) were weighted into a Pyrex tube (volume: ca. 20.0 mL with a body length of 18.0 cm, neck length of 9 cm) and to the mixture was added mesitylene (0.1 mL), 1,4-dioxane (0.9 mL) and 0.1 mL of aqueous acetic acid (6.0 mol/L). The Pyrex tube was flash frozen in a liquid nitrogen bath, evacuated to an internal pressure of ca. 19.0 mbar and flame-sealed, reducing the total length by ca. 10.0 cm. Upon warming to room temperature, the tube was placed in an oven at 120 °C for three days. As a result, an orange powder was isolated by centrifugation and washed with acetone (3 × 5.0 mL), and the yield is about 86%. Anal. Cald: C: 69.13; H: 2.88; N: 11.52; S: 13.17; O: 3.30. Found: C: 70.04; H: 2.35; N: 11.03; S: 13.01; O: 3.57.

1.3 Experimental Methods

Nuclear magnetic resonance spectroscopy (NMR)

^{1}H NMR spectra were recorded on a Avance III-400 NMR spectrometer, where chemical shifts (δ in ppm) were determined with a residual proton of the solvent as standard.

UV/Vis spectra

Solid UV/Vis spectra have been carried out on a Shimadzu Corporation U-4100 Spectrophotometer within the wavelength range 200–800 nm. liquid UV/Vis spectra have been carried out on a Shimadzu Corporation UV-2700 Spectrophotometer within the wavelength range 200–800 nm.

Infrared spectra

The FT-IR spectra (KBr) were obtained using a IFS-66V/S Fourier transform infrared spectrophotometer from Brucker Germany.

Field emission scanning electron microscopy

Field emission scanning electron microscopy was performed on a SU8020 model HITACHI microscope.

Transmission electron microscope

Transmission electron microscopy was performed on a Tecnai G2 S-Twin F20 with an accelerating voltage of 200 kV.

Powder X-ray diffraction

Powder X-ray diffraction data were recorded on a PANalytical BV Empyrean diffractometer by depositing powder on glass substrate, from 2θ = 1.5° to 40° with 0.02° increment at 25 °C.

Thermogravimetric analysis (TGA)

Thermogravimetric analysis (TGA) was recorded on a SHIMADZU DTG-60 thermal analyzer under N_2. The operational range of the instrument was from 30 °C to 800 °C at a heating rate of 10 °C min^{-1} with N_2 flow rate of 30 mL min^{-1}.

Nitrogen sorption isotherms

The sorption isotherm for N_2 was measured by using a Quantachrome Autosorb-IQ analyzer with ultrahigh-purity gas (99.999% purity). To estimate pore size distributions, nonlocal density functional theory (NLDFT) was applied to analyze the N_2 isotherm based on the model of N_2@77K on carbon with slit pores and the method of non-negative regularization.

Electrochemical measurements

The ORR catalytic activities of prepared three COFs catalysts were measured in 0.1 M KOH solution. An ink of the catalyst was prepared by mixing 5 mg of catalyst powder and 5 mg acetylene black with 225 μL of ethanol, 225 μL of H_2O, and 50 μL 5 wt% Nafion solution, and further placed in an ultrasonic bath. 6 μL of the solution was loaded onto the electrode. The RDE measurements were performed in a three-electrode, one-compartment cell at room temperature, equipped with a graphite rod counter electrode and an Ag/AgCl reference electrode. Linear sweep voltammetry (LSV) was performed O_2-saturated 0.1 M KOH at a scan rate of 10 mV s^{-1} under various electrode rotation rates (400, 625, 900, 1025, 1600, 2225 and 2500 rpm, respectively). Cyclic voltammetry (CV) was performed in N_2-saturated and O_2-saturated 0.1 M KOH at a scan rate of 50 mV s^{-1}. Preparation of a small amount of catalyst into an ethanol solution for impedance-potential testing in 0.1 mol/L Na_2SO_4 to obtain the conductivity values. A solution of the catalyst was prepared by adding 5 mg of catalyst powder into 225 μL of ethanol, 225 μL of H_2O, and 50 μL N-Methylpyrrolidone (NMP) solution of 1.5 wt% Polyvinylidene fluoride (PVDF), and further placed in an ultrasonic bath. 7 μL of the solution was

loaded onto the glassy carbon electrodes. Impedance tests were carried out in a 0.1 mol/L KCl solution containing 5 mmol/L $[Fe(CN)_6]^{3-/4-}$ at an open circuit voltage at room temperature. Multi-step chonoamperometric curve was conducted by measuring the current changes of the catalyst at each applied potential (0.3, 0.6 and 0.7 V vs. RHE) using a ring-disk electrode in O_2-saturated on a CHI 760 Eelectrochemical workstation (set to two cycles). Methanol tolerance tests were performed by chronoamperometric measurement at 0.7 V (vs RHE) at a carbon paper with an area of 1×1 cm^2 (methanol was dropped into the electrolytes at 200 s).

The turnover frequency (TOF) value is calculated according to the following equation:

$$TOF = (J \times A) / (4 \times F \times n)$$

where J is the current density at a given potential, A is the surface area of the electrode (0.0707 cm^2), the number of 4 represents 4 electrons/mol of O_2, F is the Faraday constant (96485.3 C/mol), and n stands for the number of moles of Se (O or S) atoms in samples.

The Tafel slope was estimated by linear fitting of the polarization curves according to the following Tafel equation:

$$h = b \times \log j + a$$

where j is the current density and b is the Tafel slope.

The electron transfer number (n) and the faradaic efficiency of H_2O_2 can be calculated from the following equations:

$$n=4\times \frac{I_D}{I_D+I_R/N}$$

$$F_{H2O2}= \frac{I_R}{N\times I_D} \times 100\%$$

where I_D is the disk current, I_R is the ring current, and N is the collection efficiency (0.47).

Computational Details

All the calculations were performed by using the Vienna Ab initio simulation package (VASP) based on the density functional theory.[2] The generalized gradient approximation with Perdew-Burke-Ernzerhof (PBE) functional was adopted to describe the exchange and correlation potential energy.[3-5] The K-point is generated by the Monkhorst-Pack grid method with 1 × 1 × 1 for geometry optimization and 3 × 3 × 1 for electronic structure calculation.[6] The cut-off energy of plane wave basis is set as 450 eV, and the convergence criteria of the total energy and the force on each ion are 10-5 eV and 0.03 eV/Å, respectively.[7] A vacuum slab of 15 Å in the z-direction is used to avoid the interaction between period layers. Multiwfn software package was used to calculate orbital-weighted fukui functions.[8] Calculation of density of states and differential charges using the

plane wave basis set with an energy cutoff of 500 eV, the projector augmented wave (PAW) pseudopotentials, and the generalized gradient approximation parameterized by Perdew, Burke, and Ernzerhof (GGA-PBE) for exchange-correlation functional.[9, 10] A vacuum space of 20 Å was applied for the vertical direction of COF. The Brillouin zone was sampled by the Gamma point. All the model structures were fully optimized by ionic and electronic degrees of freedom using the convergence criteria of 10–4 eV for total energy and 10–2 eV/Å for the forces on each atom.

The ORR in alkaline electrolyte involves four reaction steps proposed by Nørskov *et al*, the four-electron transfer mechanism was considered with each reaction step as follows:[11]

$^{*} + O_2 \rightarrow O_2^{*}$

$O_2^{*} + H_2O\ (l) + e^{-} \rightarrow {}^{*}HOO + OH^{-}$

$^{*}HOO + e^{-} \rightarrow O^{*} + OH^{-}$

$^{*}O + H_2O\ (l) + e^{-} \rightarrow HO^{*} + OH^{-}$

$HO^{*} + e^{-} \rightarrow OH^{-} + {}^{*}$

where * represents the chemisorption site and *OOH, *O, *OH are the reaction oxygen intermediate species. The reaction free energy (ΔG) of each step is calculated by $\Delta G = \Delta E + \Delta ZPE - T\Delta S + \Delta GU$

where ΔE and ΔZPE represent the adsorption energy of oxygen intermediate species obtained by DFT calculation and the zero-point energy. $T\Delta S$ is the change in entropy contribution to the free energy, U is the applied potential. Each step of was obtained as follows:

$\Delta G_1 = \Delta G_{OOH^*} - eU + \Delta G_{H+} - 4.92eV$

$\Delta G_2 = \Delta G_{O^*} - \Delta G_{OOH^*} - eU + \Delta G_{H+}$

$\Delta G_3 = \Delta G_{OH^*} - \Delta GO^* - eU + \Delta G_{H+}$

$\Delta G_4 = -\Delta G_{OH^*} - eU + \Delta G_{H+}$

2. Results and Discussion

2.1. Additional Supplementary Figures

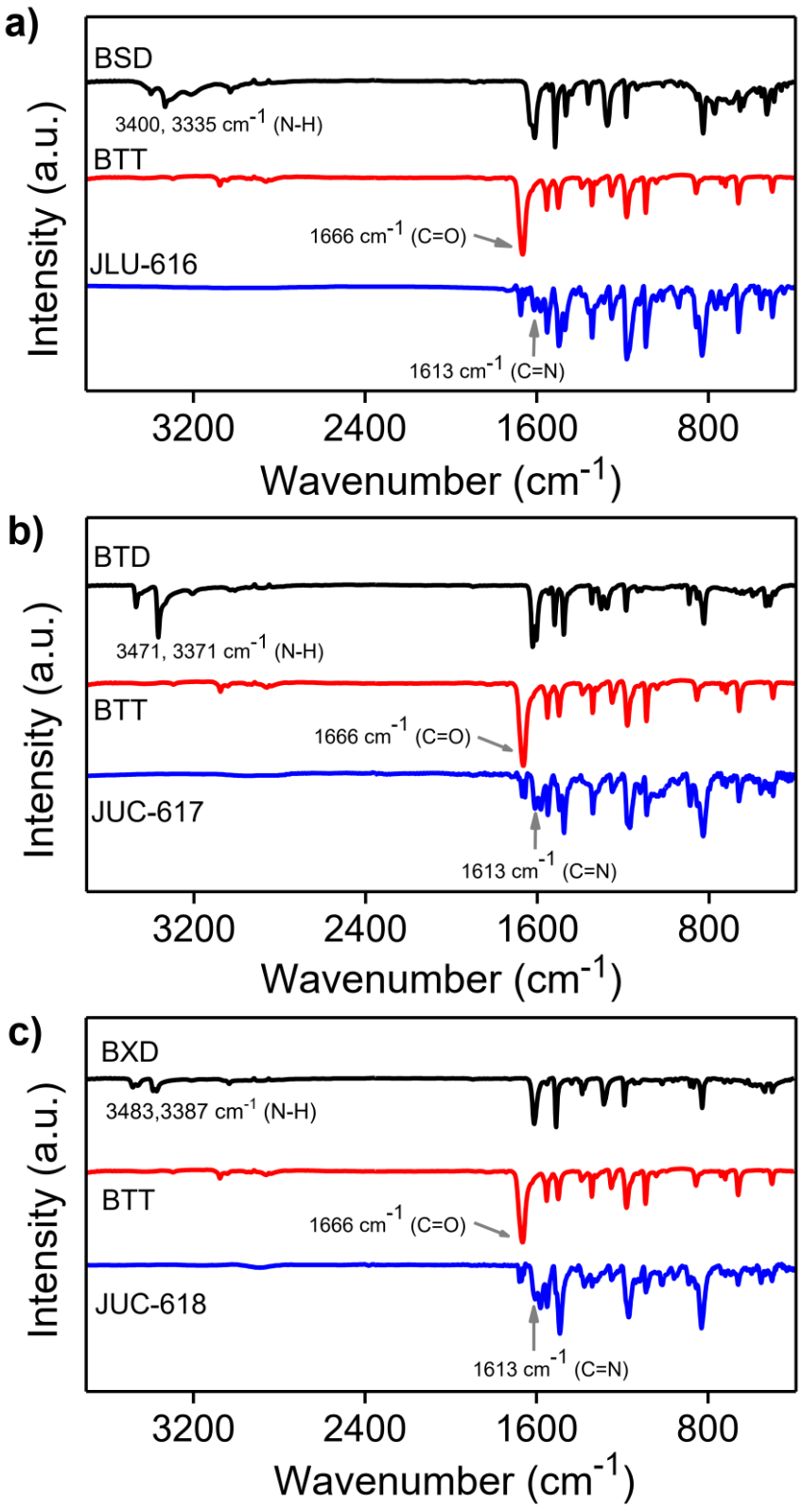

Figure S1. (a) FT-IR spectra of JUC-616 and corresponding monomers. (b) FT-IR spectra of JUC-617 and corresponding monomers. (c) FT-IR spectra of JUC-618 and corresponding monomers.

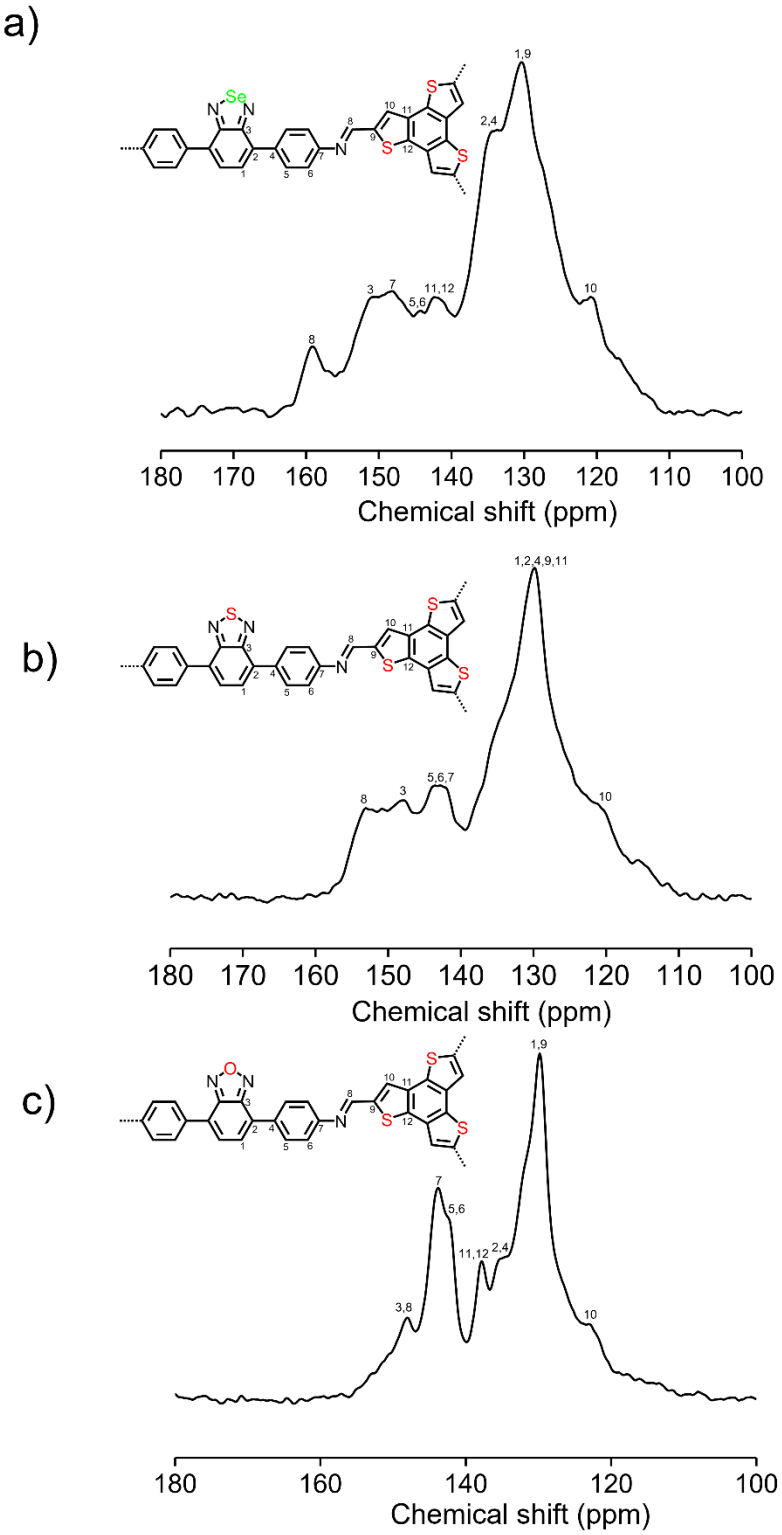

Figure S2. Solid state ^{13}C NMR of JUC-616 (a), JUC-617 (b) and JUC-618 (c).

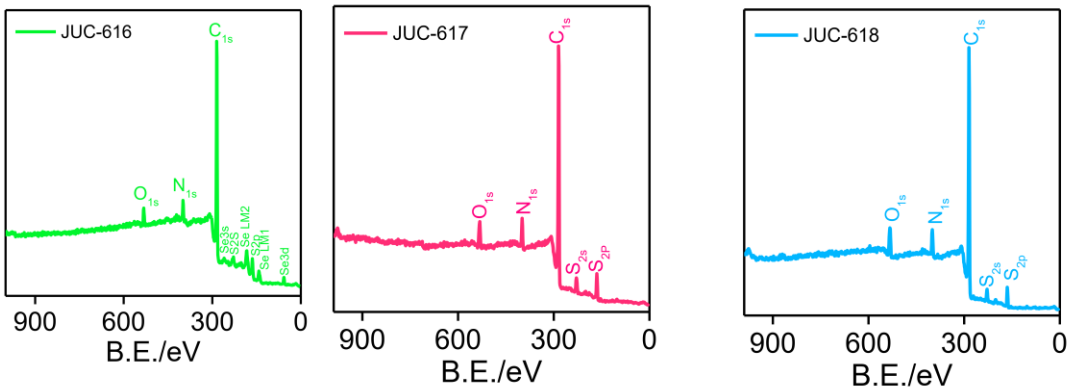

Figure S3. XPS survey spectra of JUC-616 (a), JUC-617 (b) and JUC-618 (c). [12, 13]

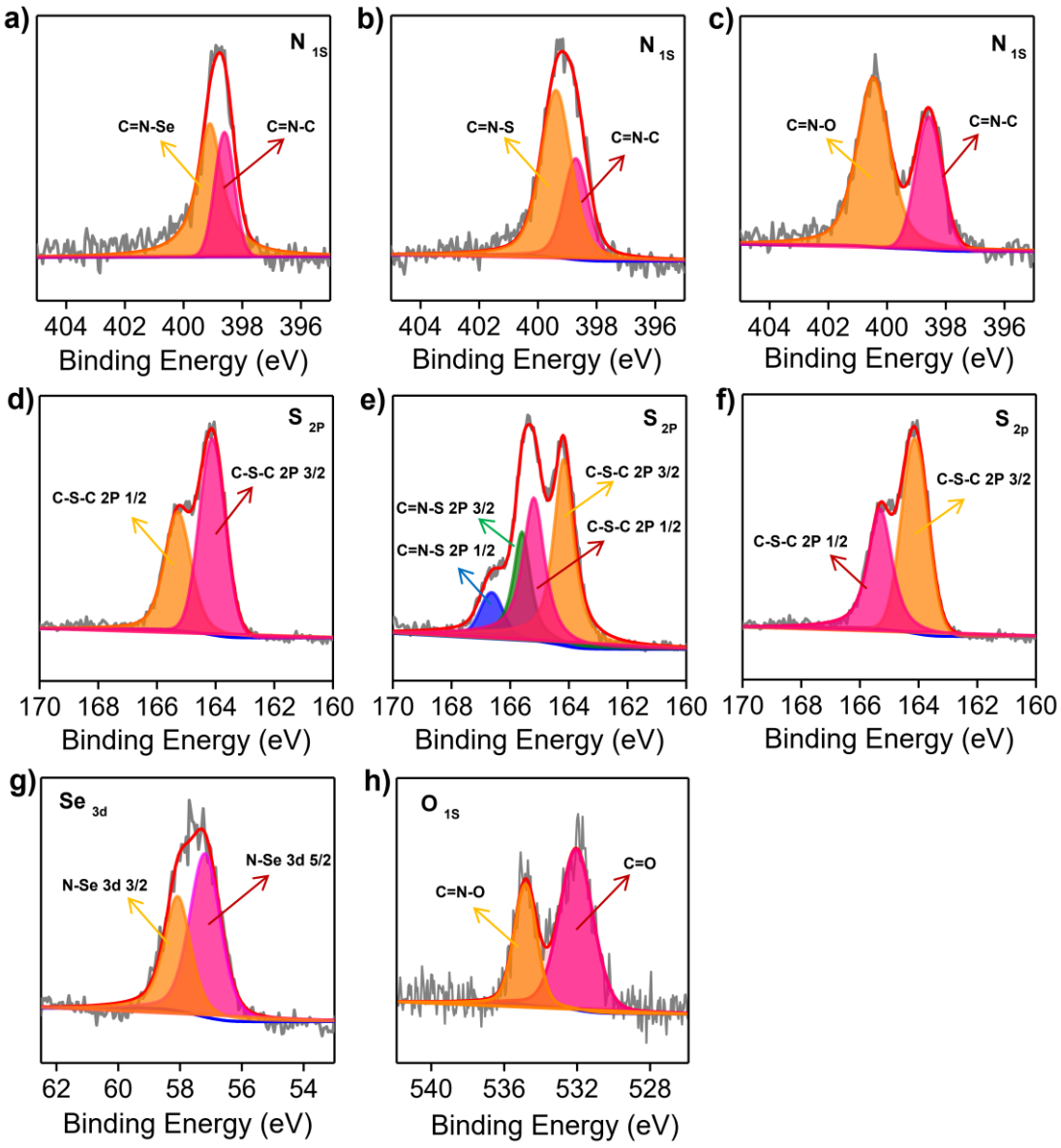

Figure S4. N 1s XPS spectra of JUC-616 (a), JUC-617 (b) and JUC-618 (c). S 2p XPS spectra FT-IR spectra of JUC-616 (d), JUC-617 (e) and JUC-618 (f). Se 3d XPS spectrum of JUC-616 (g). O 1s XPS spectrum of JUC-618 (h).

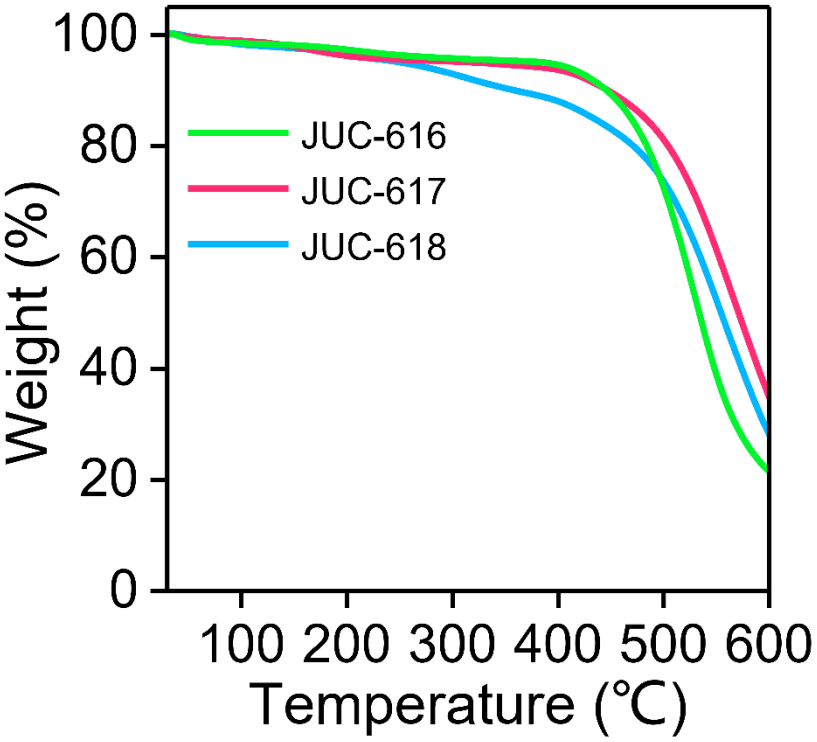

.

Figure S5. TGA curves of JUC-616 (green), JUC-617 (red) and JUC-618 (blue).

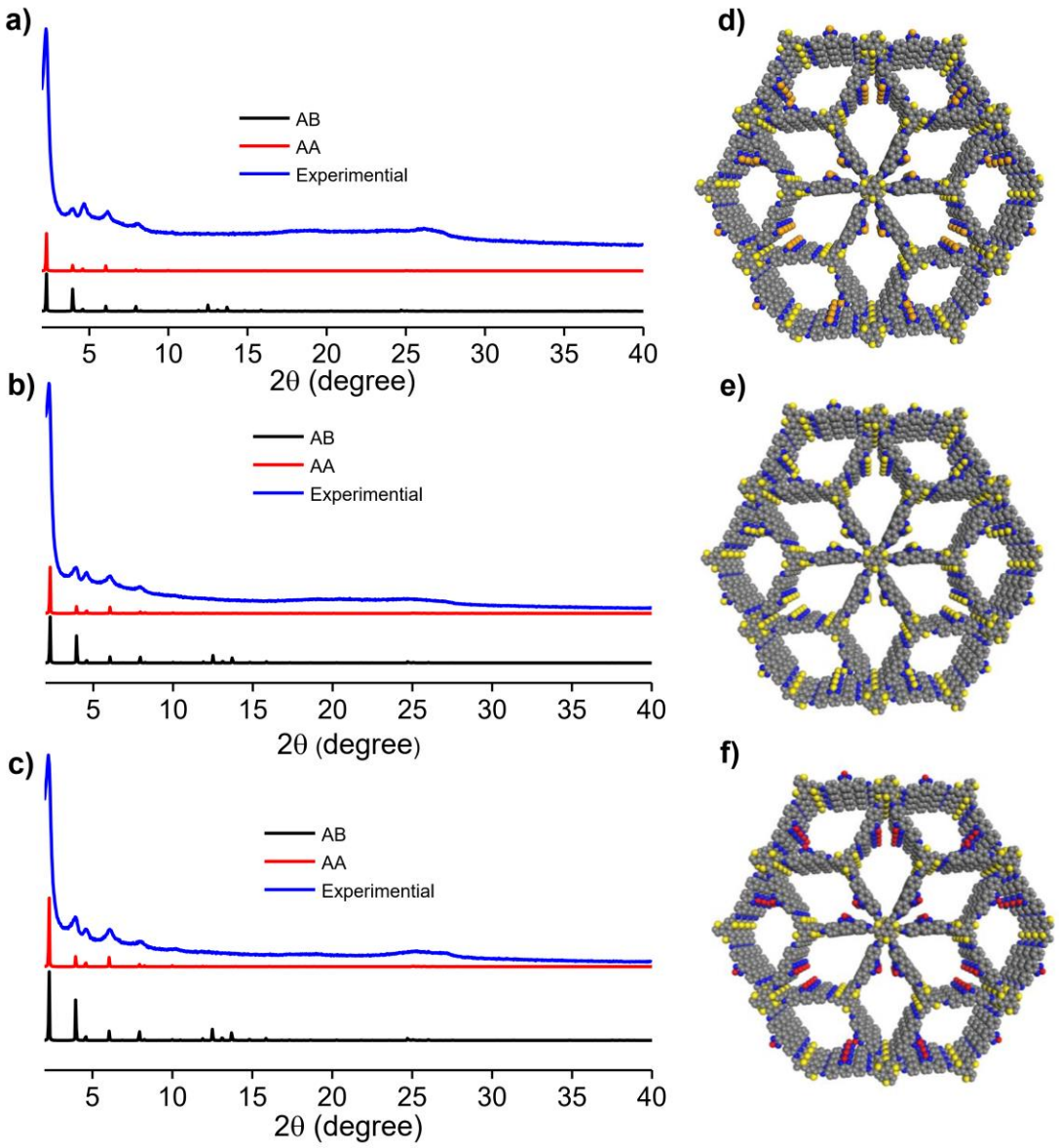

Figure S6. XRD profiles of JUC-616 (a), JUC-617 (b) and JUC-618 (c). Experimentally observed (blue line), simulated by using AA-stacking (red line) and AB-stacking (black line) models. Crystal structures of the AB stacking model for JUC-616 (d), JUC-617 (e) and JUC-618 (f).

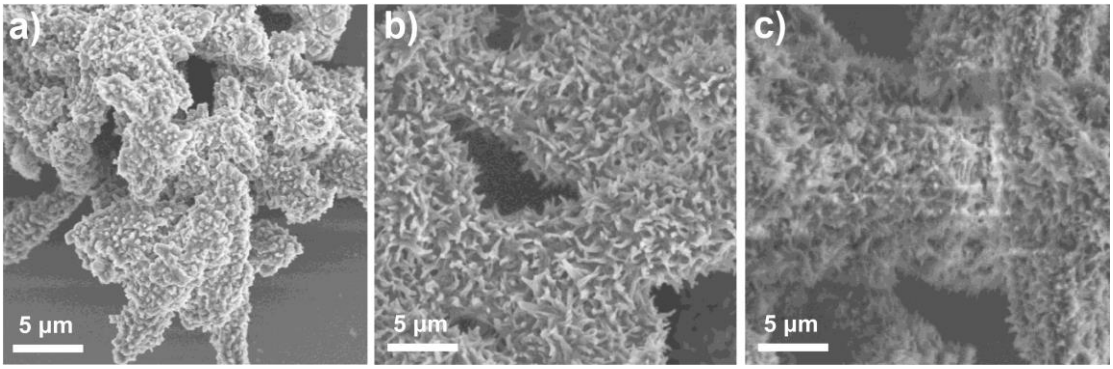

Figure S7. FE-SEM images of JUC-616 (a), JUC-617 (b) and JUC-618 (c).

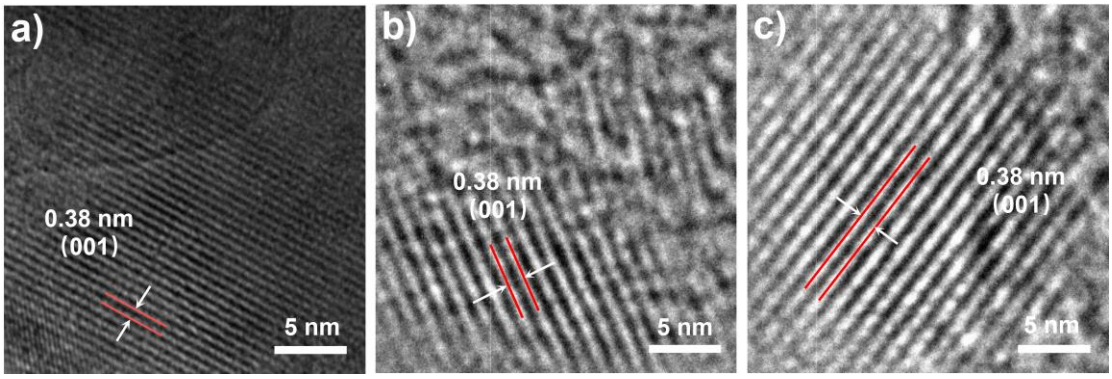

Figure S8. HR-TEM images of JUC-616 (a), JUC-617 (b) and JUC-618 (c).

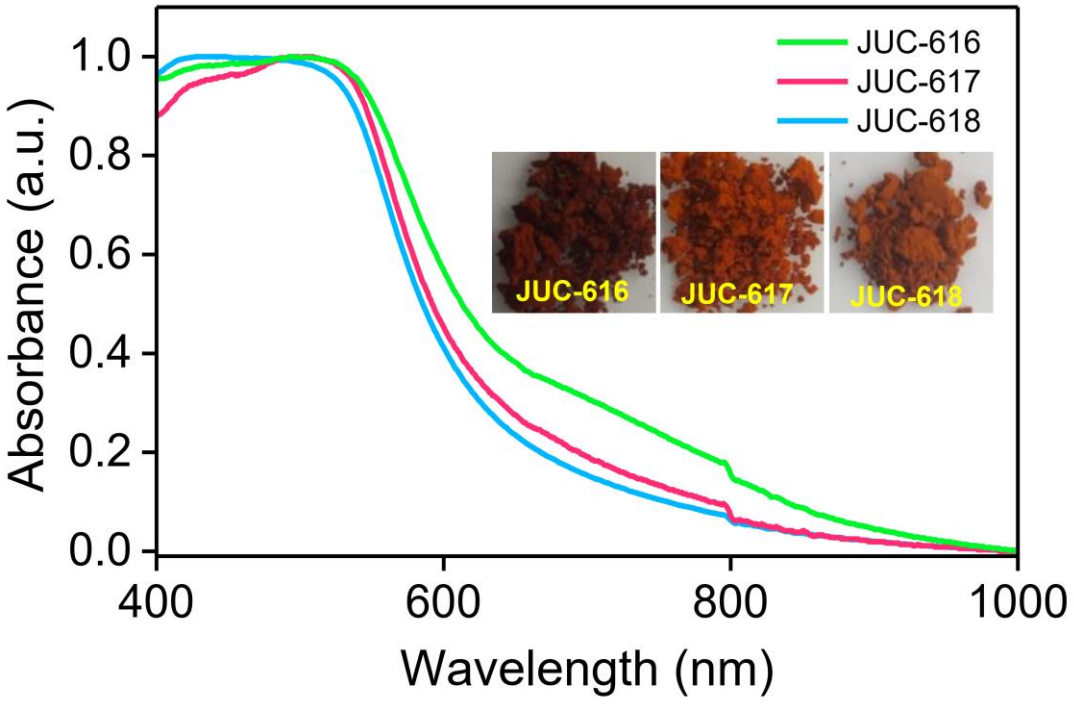

Figure S9. UV-Vis diffuse reflectance spectra of JUC-616, JUC-617 and JUC-618. Insets: their optical images.

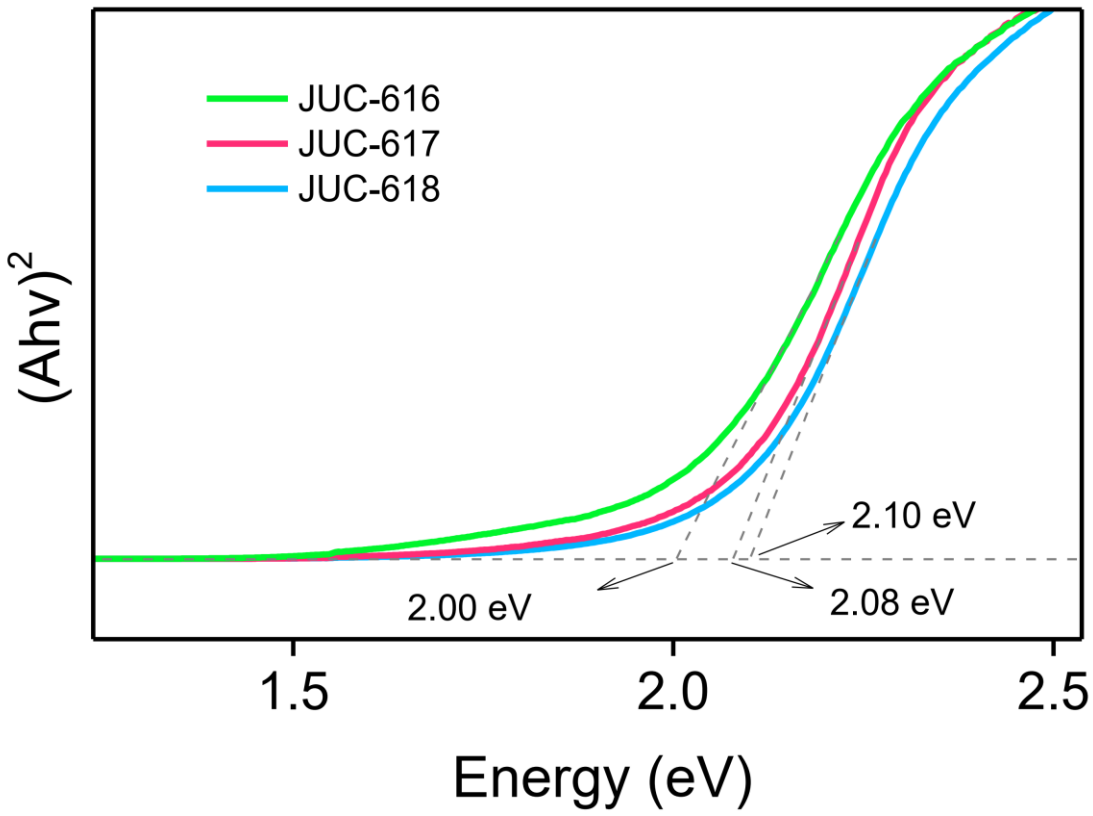

Figure S10. Tauc plots of JUC-616, JUC-617 and JUC-618.

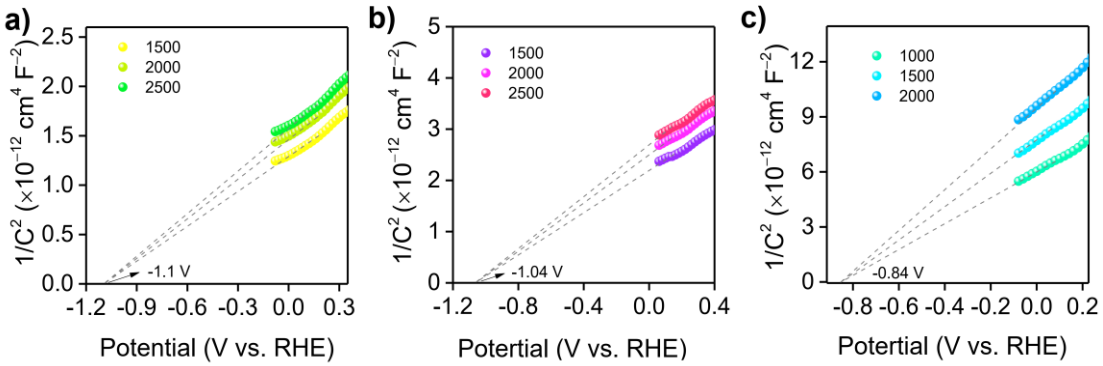

Figure S11. Mott-Schottky curves of JUC-616 (a), JUC-617 (b) and JUC-618 (c) in 0.1 M Na_2SO_4 aqueous solution at three different frequencies.

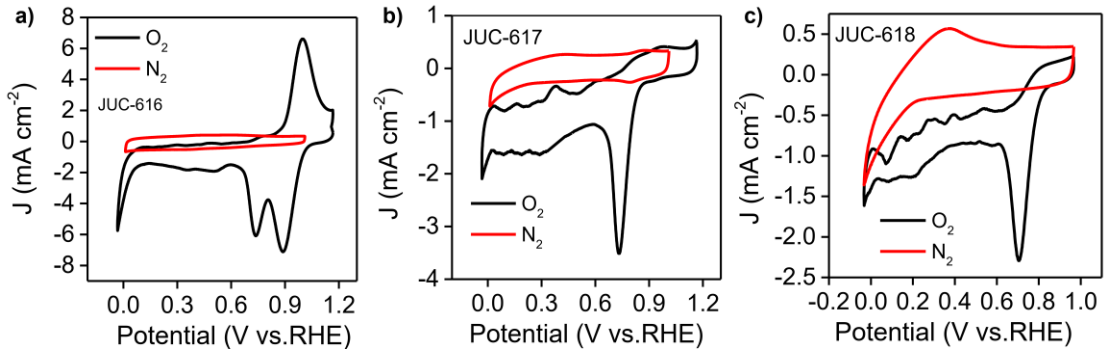

Figure S12. Cyclic voltammetric curves of JUC-616 (a), JUC-617 (b) and JUC-618 (c) under N_2 (red line) and O_2 (black line). Note: Under O_2-saturated conditions, JUC-616 shows a pair of redox peaks near 0.9 V vs. RHE, which corresponds to LSV. Oxygen combines with Se to form Se=O,[14] and the larger hybrid orbital and longer bond length of Se=O results in a weaker π overlap, reducing the π-bonding nature of the Se=O bond, causing Se=O to be readily reduced to lower valence Se.[15]

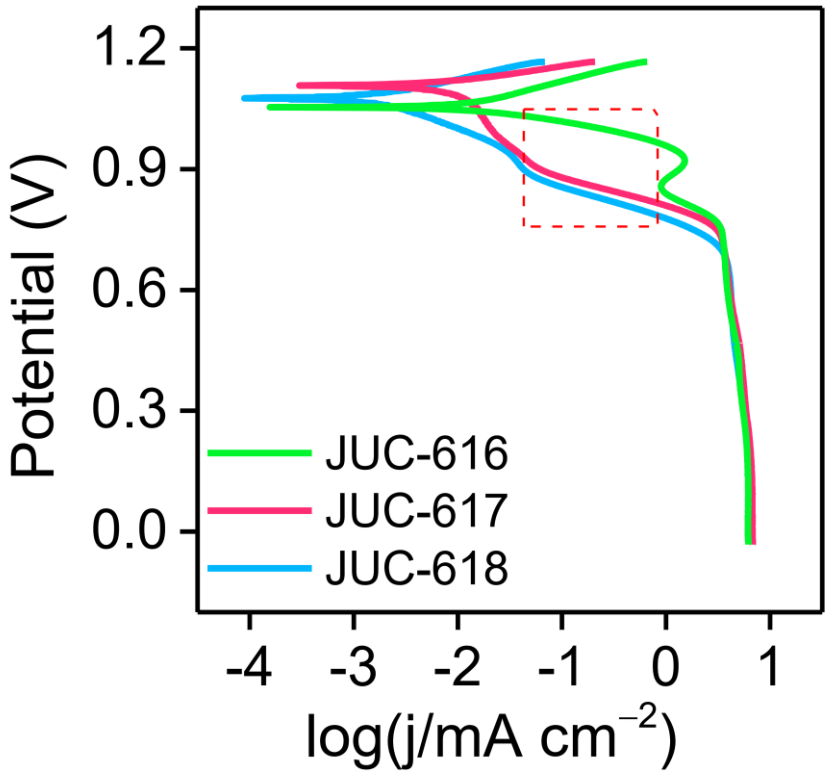

Figure S13. The full plot of tafel slope of JUC-616, JUC-617 and JUC-618.

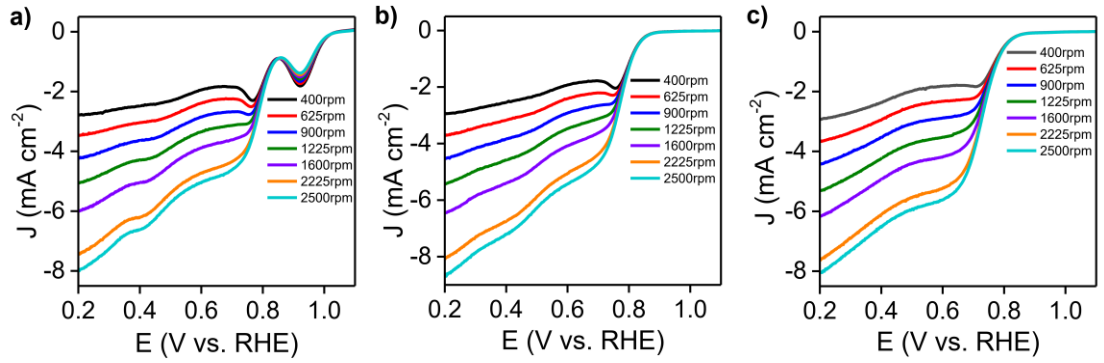

Figure S14. LSV curves of JUC-616 (a), JUC-617 (b) and JUC-618 (c) at various rotation speeds.

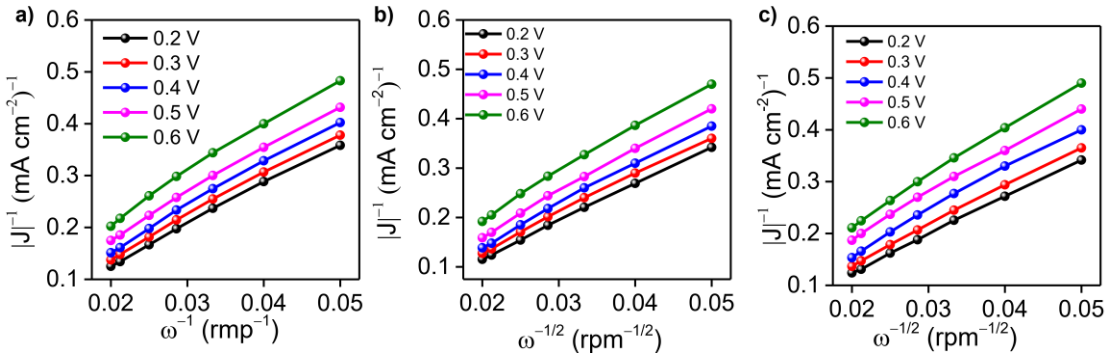

Figure S15. The K-L plots forJUC-616 (a), JUC-617 (b), and JUC-618 (c) at 0.2 V~0.6 V (vs RHE).

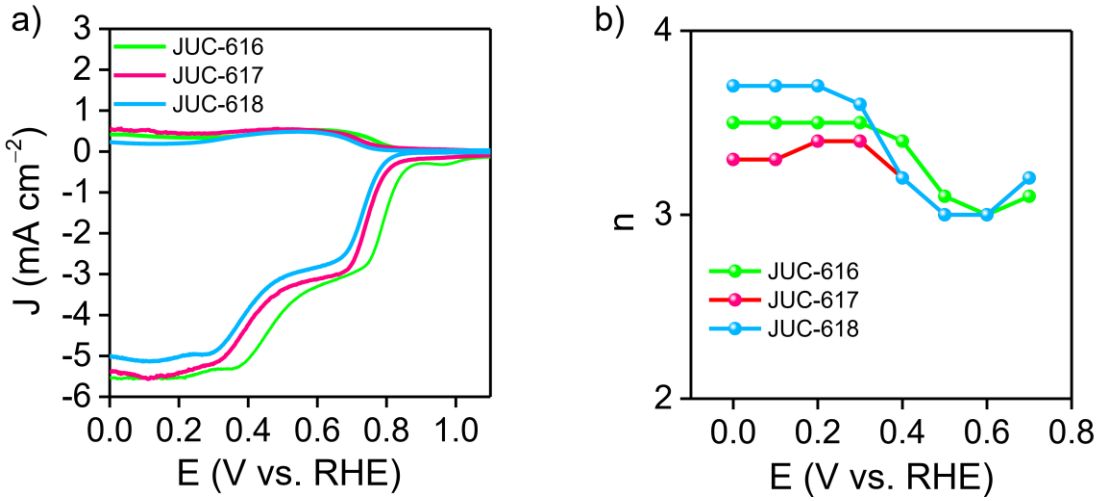

Figure S16. RRDE voltammogram (a) and electrons transfer (n) (b) of JUC-616, JUC-617 and JUC-618 in O_2 saturated 0.1 M KOH.

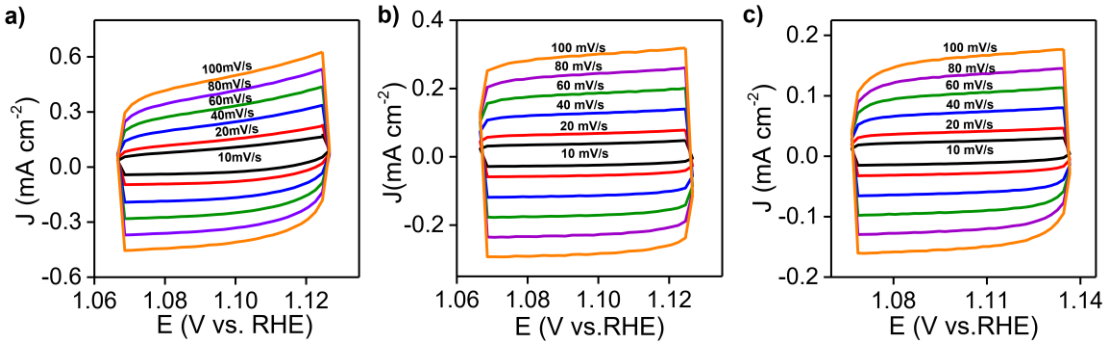

Figure S17. Cyclic voltammetric curves of JUC-616 (a), JUC-617 (b) and JUC-618 (c) in 0.1 M KOH solution

at different scan rates (10, 20, 40, 60, 80 and 100 mV s^{-1}).

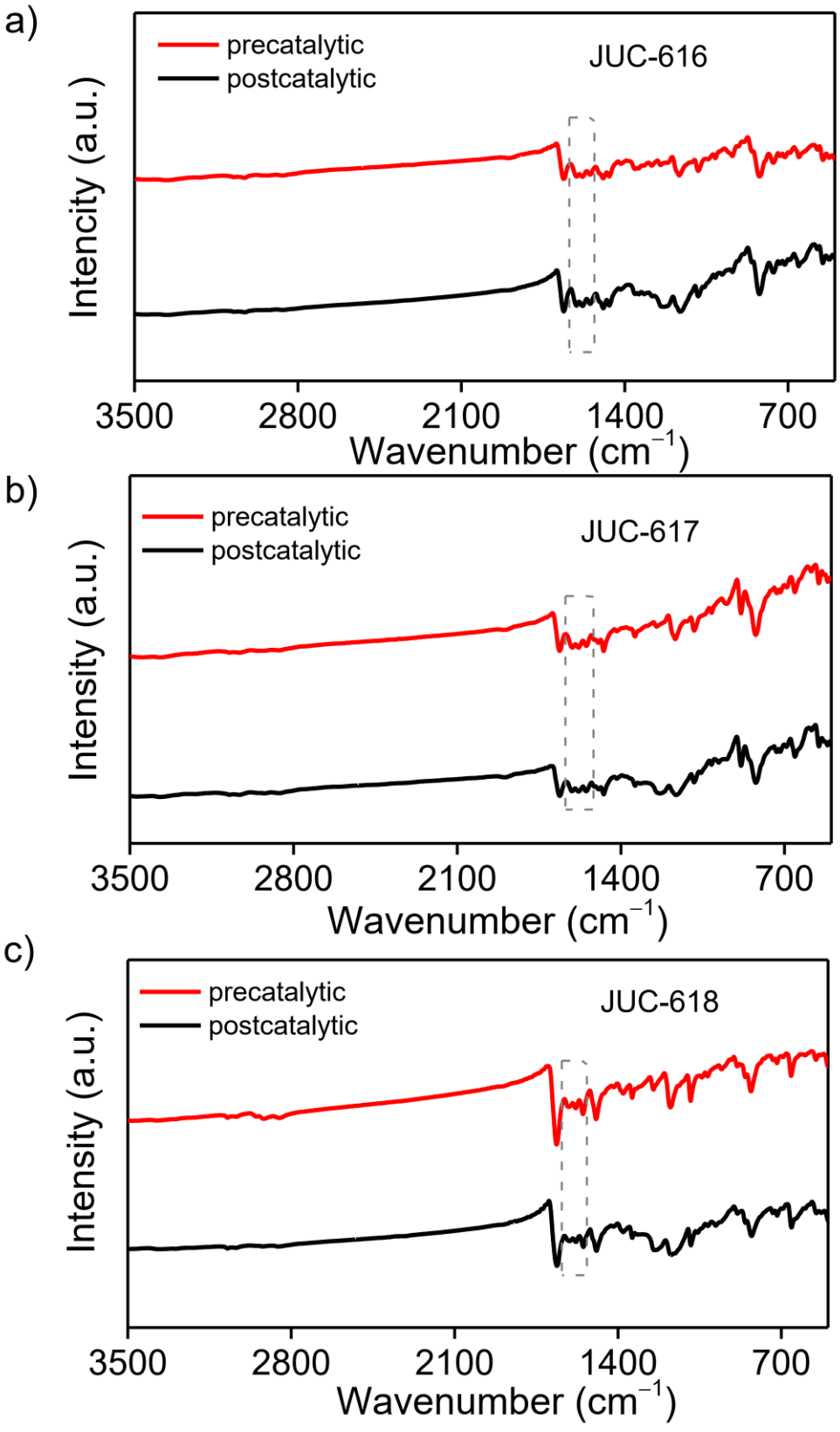

Figure S18. FT-IR spectra of JUC-616 (a), JUC-617 (b) and JUC-618 (c) before and after electrocatalysis.

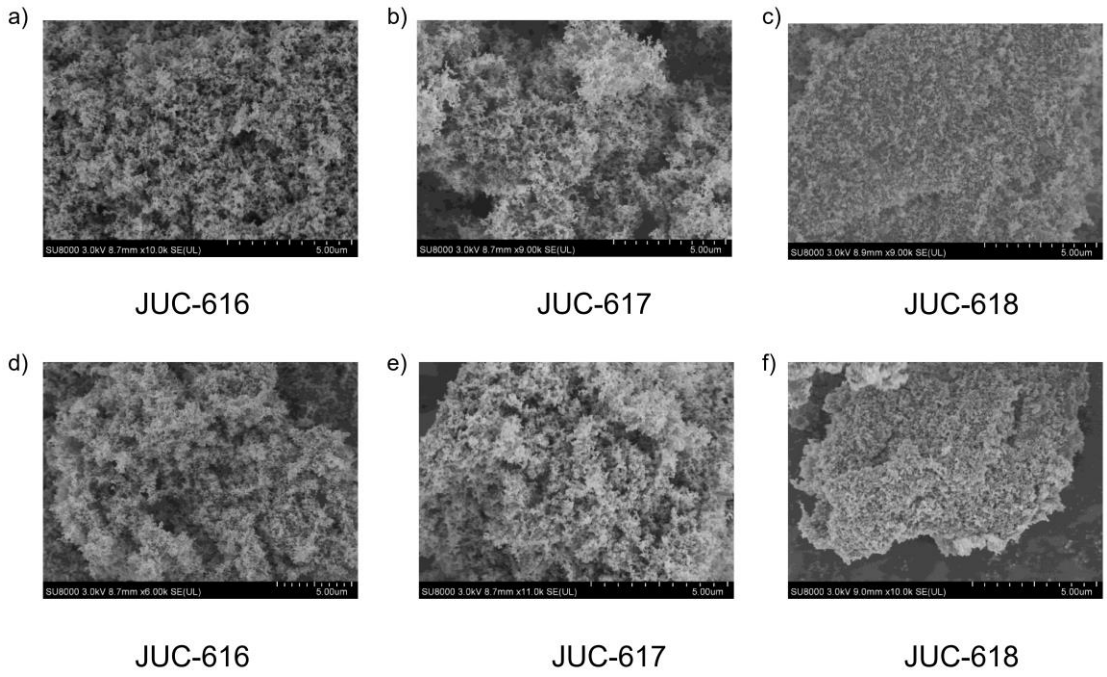

Figure S19. FE-SEM images of JUC-616 (a), JUC-617 (b) and JUC-618 (c) before electrocatalysis, and JUC-616 (d), JUC-617 (e) and JUC-618 (f) after electrocatalysis.

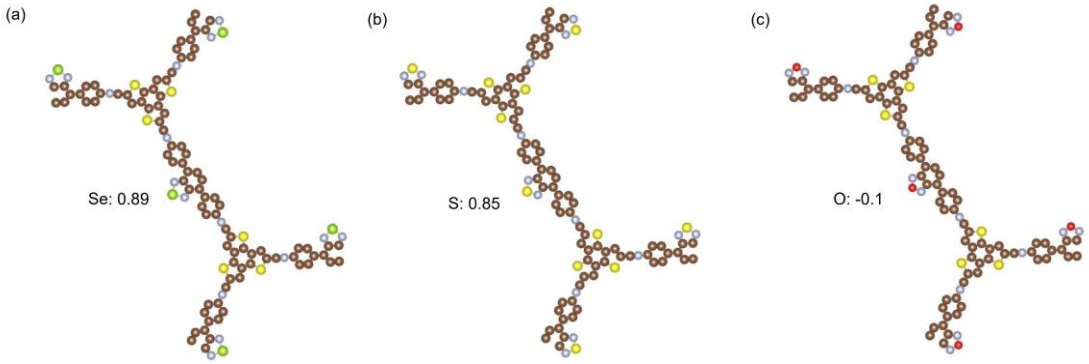

Figure S20. The mulliken charge distribution model of JUC-616, JUC-617 and JUC-618.

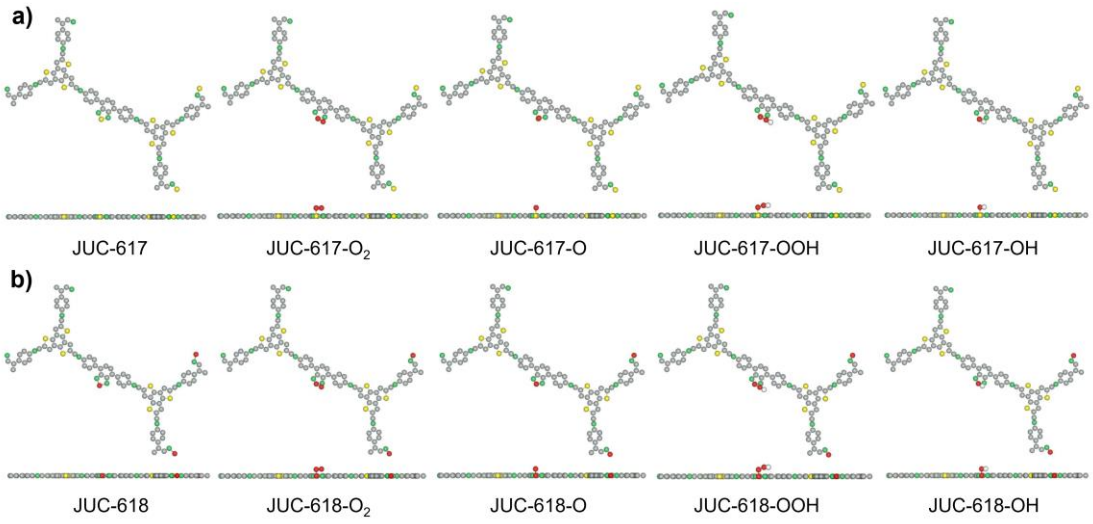

Figure S21. Models of the adsorption intermediate state of JUC-617 (a) and JUC-618 (b).

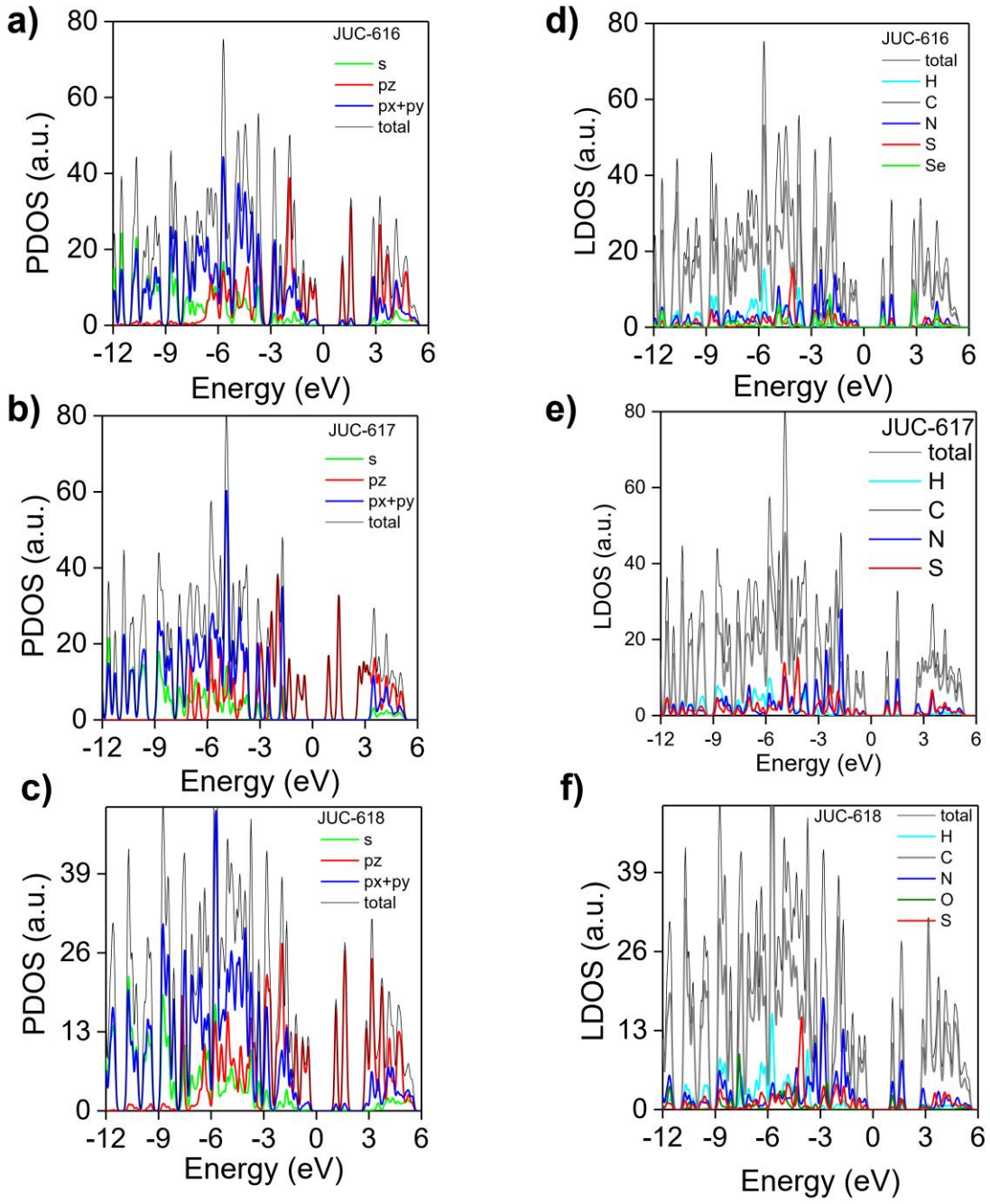

Figure S22. Partial density of states for JUC-616 (a), JUC-617 (b) and JUC-618 (c). Local density of states for JUC-616 (d), JUC-617 (e) and JUC-618 (f).

2.2. Additional Supplementary Tables

Table S1. Unit cell parameters and fractional atomic coordinates for JUC-616.

Space group		*P*-6	
Observed cell parameters		$a = b = 44.5787$ Å and $c = 3.5618$ Å $\alpha = \beta = 90°$, $\gamma = 120°$	
Simulated cell parameters		$a = b = 44.6085$ Å and $c = 3.5302$ Å $\alpha = \beta = 90°$, $\gamma = 120°$	
Agreement factors		$R_{wp} = 3.23\%$, $R_p = 2.45\%$	
atoms	x	y	z
C1	0.36395	0.66286	0.5
C2	0.38965	0.65458	0.5
C3	0.44111	0.57281	0.5
C4	0.46039	0.55594	0.5
C5	0.52228	0.50739	0.5
C6	0.63384	0.33306	0.5
C7	0.60566	0.33758	0.5
C8	0.54109	0.40734	0.5
C9	0.51861	0.42064	0.5
C10	0.45061	0.46579	0.5
C11	0.66607	0.36586	0.5
S12	0.66048	0.40090	0.5
C13	0.59009	0.46554	0.5
C14	0.56753	0.47875	0.5
C15	0.50132	0.52249	0.5
C16	0.32983	0.63223	0.5
S17	0.33067	0.59451	0.5
C18	0.38818	0.51744	0.5
C19	0.40754	0.50065	0.5
C20	0.47137	0.45083	0.5
C21	0.37537	0.61891	0.5
N22	0.38424	0.57001	0.5
C23	0.39748	0.60332	0.5
C24	0.44390	0.51958	0.5
C25	0.40479	0.55356	0.5
C26	0.46501	0.50210	0.5
C27	0.61631	0.37259	0.5
N28	0.60083	0.41705	0.5
C29	0.59100	0.38436	0.5
C30	0.53144	0.45652	0.5
C31	0.57706	0.42981	0.5
C32	0.50786	0.47124	0.5
N33	0.45368	0.41601	0.5
O34	0.40779	0.39901	0.5
N35	0.41645	0.44283	0.5
H36	0.41797	0.67599	0.5
H37	0.45489	0.60231	0.5
H38	0.48989	0.57167	0.5
H39	0.55161	0.52502	0.5
H40	0.57842	0.31409	0.5
H41	0.53022	0.37812	0.5
H42	0.48940	0.40229	0.5
H43	0.61929	0.48395	0.5
H44	0.57832	0.50795	0.5
H45	0.51423	0.55195	0.5
H46	0.35868	0.50164	0.5
H47	0.50164	0.47115	0.5
H48	0.42686	0.62056	0.5
H49	0.56211	0.36464	0.5

Table S2. Unit cell parameters and fractional atomic coordinates for JUC-617.

Space group		*P*-6	
Observed cell parameters		$a = b = 44.5787$ Å and $c = 3.5618$ Å $\alpha = \beta = 90°$, $\gamma = 120°$	
Simulated cell parameters		$a = b = 44.5873$ Å and $c = 3.5439$ Å $\alpha = \beta = 90°$, $\gamma = 120°$	
Agreement factors		R_{wp} = 3.09%, R_p = 2.19%	
atoms	x	y	z
C1	0.36395	0.66286	0.5
C2	0.38965	0.65458	0.5
C3	0.44111	0.57281	0.5
C4	0.46039	0.55594	0.5
C5	0.52228	0.50739	0.5
C6	0.63384	0.33306	0.5
C7	0.60566	0.33758	0.5
C8	0.54109	0.40734	0.5
C9	0.51861	0.42064	0.5
C10	0.45061	0.46579	0.5
C11	0.66607	0.36586	0.5
S12	0.66048	0.40090	0.5
C13	0.59009	0.46554	0.5
C14	0.56753	0.47875	0.5
C15	0.50132	0.52249	0.5
C16	0.32983	0.63223	0.5
S17	0.33067	0.59451	0.5
C18	0.38818	0.51744	0.5
C19	0.40754	0.50065	0.5
C20	0.47137	0.45083	0.5
C21	0.37537	0.61891	0.5
N22	0.38424	0.57001	0.5
C23	0.39748	0.60332	0.5
C24	0.44390	0.51958	0.5
C25	0.40479	0.55356	0.5
C26	0.46501	0.50210	0.5
C27	0.61631	0.37259	0.5
N28	0.60083	0.41705	0.5
C29	0.59100	0.38436	0.5
C30	0.53144	0.45652	0.5
C31	0.57706	0.42981	0.5
C32	0.50786	0.47124	0.5
N33	0.45368	0.41601	0.5
S34	0.40779	0.39901	0.5
N35	0.41645	0.44283	0.5
H36	0.41797	0.67599	0.5
H37	0.45489	0.60231	0.5
H38	0.48989	0.57167	0.5
H39	0.55161	0.52502	0.5
H40	0.57842	0.31409	0.5
H41	0.53022	0.37812	0.5
H42	0.48940	0.40229	0.5
H43	0.61929	0.48395	0.5
H44	0.57832	0.50795	0.5
H45	0.51423	0.55195	0.5
H46	0.35868	0.50164	0.5
H47	0.50164	0.47115	0.5
H48	0.42686	0.62056	0.5
H49	0.56211	0.36464	0.5

Table S3. Unit cell parameters and fractional atomic coordinates for JUC-618.

Space group		*P*-6	
Observed cell parameters		$a = b = 44.5787$ Å and $c = 3.5618$ Å $\alpha = \beta = 90°$, $\gamma = 120°$	
Simulated cell parameters		$a = b = 44.5786$ Å and $c = 3.5617$ $\alpha = \beta = 90°$, $\gamma = 120°$	
Agreement factors		$R_{wp} = 1.57\%$, $R_p = 1.17\%$	
atoms	x	y	z
C1	0.36395	0.66286	0.5
C2	0.38965	0.65458	0.5
C3	0.44111	0.57281	0.5
C4	0.46039	0.55594	0.5
C5	0.52228	0.50739	0.5
C6	0.63384	0.33306	0.5
C7	0.60566	0.33758	0.5
C8	0.54109	0.40734	0.5
C9	0.51861	0.42064	0.5
C10	0.45061	0.46579	0.5
C11	0.66607	0.36586	0.5
S12	0.66048	0.40090	0.5
C13	0.59009	0.46554	0.5
C14	0.56753	0.47875	0.5
C15	0.50132	0.52249	0.5
C16	0.32983	0.63223	0.5
S17	0.33067	0.59451	0.5
C18	0.38818	0.51744	0.5
C19	0.40754	0.50065	0.5
C20	0.47137	0.45083	0.5
C21	0.37537	0.61891	0.5
N22	0.38424	0.57001	0.5
C23	0.39748	0.60332	0.5
C24	0.44390	0.51958	0.5
C25	0.40479	0.55356	0.5
C26	0.46501	0.50210	0.5
C27	0.61631	0.37259	0.5
N28	0.60083	0.41705	0.5
C29	0.59100	0.38436	0.5
C30	0.53144	0.45652	0.5
C31	0.57706	0.42981	0.5
C32	0.50786	0.47124	0.5
N33	0.45368	0.41601	0.5
Se34	0.40779	0.39901	0.5
N35	0.41645	0.44283	0.5
H36	0.41797	0.67599	0.5
H37	0.45489	0.60231	0.5
H38	0.48989	0.57167	0.5
H39	0.55161	0.52502	0.5
H40	0.57842	0.31409	0.5
H41	0.53022	0.37812	0.5
H42	0.48940	0.40229	0.5
H43	0.61929	0.48395	0.5
H44	0.57832	0.50795	0.5
H45	0.51423	0.55195	0.5
H46	0.35868	0.50164	0.5
H47	0.50164	0.47115	0.5
H48	0.42686	0.62056	0.5
H49	0.56211	0.36464	0.5

Table S4. Metal-free organic porous materials without pyrolysis of ORR reactions.

COFs	$E_{1/2}$ (V)	J_{lim} (mA cm^{-2})	Tafel	Cdl	Ref.
H-TP-COF	0.65	~2.5	104	2.1	*Chem. Commun.* **2021**, *57*, 12619-12622.
JUC-528	0.7	5	65.9	7.6	*J. Am. Chem. Soc.* **2020**, *142*, 8104.
TZA-COF	~0.75	3.5	67.1	-	*Nanoscale* **2020**, *12*, 22718.
TAPTt	0.74	6.21	158	-	*ACS Nano* **2021**, *15*, 3309.
PTCOF	~0.7	~4.5	124	-	*Adv. Funct. Mater.* **2021**, *31*, 2101727.
TTF-F	0.767	6.15	-	-	*Adv. Mater.* **2015**, *27*, 3190.
TTF-B	~0.72	~5	-	-	*Adv. Mater.* **2015**, *27*, 3190.
PTM-H-COF@C	0.62	2.5	-	-	*Angew. Chem. Int. Ed.* **2018**, *57*, 8007
PTM-CORF@C	0.70	6	-	-	*Angew. Chem. Int. Ed.* **2018**, *57*, 8007
TAPA-NDI-Super P	~0.71	6	76.4	-	*Appl. Mater. Today* **2022**, *26*, 101384
DAPT-TFP-COF/GC	~0.67	~4.5	-	-	*Nano Res.* **2022**, *15,* 3907
Azo-COF	0.68	5.43	89	1.73	*Angew. Chem. Int. Ed. 2022, 61, e202209583*
DAF-COF	0.74	~5	65.1	5.78	*Adv. Mater. 2023, 35, 2209129*
COF-JLU82	0.68	~5	72.79	2.38	*Macromol. Rapid Commun. 2022, 2200717*
JUC-618	0.71	6.17	78.96	3.12	This work
JUC-617	0.74	6.48	75.40	5.80	This work
JUC-616	**0.78**	**6.01**	**52.91**	**8.62**	**This work**

Table S5. Electron transfer number of JUC-616,JUC-617 and JUC-618 at different potentials.

	0.2 V	**0.3 V**	**0.4 V**	**0.5 V**	**0.6 V**
JUC-616	3.6	3.5	3.3	3.3	3.0
JUC-617	3.7	3.6	3.4	3.2	3.0
JUC-618	3.9	3.7	3.4	3.3	3.0

Table S6. Charge distribution of JUC-616, JUC-617 and JUC-618.

Mulliken Charge			
	JUC-616	**JUC-617**	**JUC-618**
C1	-0.03	-0.03	-0.03
C2	-0.03	-0.03	-0.03
C3	-0.03	-0.03	-0.03
C4	-0.11	-0.11	-0.1
C5	-0.11	-0.11	-0.1
C6	-0.11	-0.1	-0.1
C7	-0.01	-0.01	-0.01
C8	-0.02	-0.02	-0.01
C9	-0.01	-0.01	-0.01
C10	0.02	0.02	0.02
C11	0.01	0.02	0.01
C12	0.02	0.02	0.02
C13	0.03	0.03	0.03
C14	0.03	0.03	0.03
C15	0.03	0.03	0.03
C16	-0.03	-0.03	-0.03
C17	-0.03	-0.03	-0.03
C18	-0.03	-0.03	-0.03
C19	-0.11	-0.1	-0.1
C20	-0.11	-0.1	-0.1
C21	-0.11	-0.1	-0.1

C22	-0.06	-0.05	-0.04
C23	-0.06	-0.05	-0.04
C24	-0.06	-0.05	-0.04
C25	0.07	0.07	0.07
C26	0.07	0.07	0.07
C27	0.07	0.07	0.07
C28	0.15	0.16	0.16
C29	0.15	0.15	0.16
C30	0.15	0.15	0.16
C31	-0.14	-0.15	-0.15
C32	-0.14	-0.14	-0.15
C33	-0.14	-0.14	-0.15
C34	-0.02	-0.02	-0.02
C35	-0.03	-0.03	-0.02
C36	-0.03	-0.03	-0.02
C37	0.02	0.02	0.02
C38	0.02	0.02	0.02
C39	0.02	0.02	0.02
C40	0.03	0.03	0.04
C41	0.03	0.03	0.04
C42	0.03	0.03	0.03
C43	-0.15	-0.15	-0.15
C44	-0.14	-0.15	-0.15
C45	-0.15	-0.15	-0.15
C46	-0.07	-0.06	-0.05
C47	-0.07	-0.06	-0.04
C48	-0.07	-0.06	-0.05
C49	0.06	0.07	0.06
C50	0.06	0.07	0.07
C51	0.06	0.07	0.07
C52	0.15	0.16	0.16
C53	0.15	0.16	0.16
C54	0.15	0.15	0.16
C55	-0.27	-0.27	-0.27
C56	-0.27	-0.27	-0.27
C57	-0.27	-0.27	-0.27
C58	0.46	0.46	0.46
C59	0.46	0.46	0.46
C60	0.46	0.46	0.46
C61	-0.07	-0.07	-0.07
C62	-0.07	-0.07	-0.07
C63	-0.07	-0.07	-0.07
C64	0.06	0.06	0.06
C65	0.06	0.06	0.06
C66	0.06	0.06	0.06
C67	-0.04	-0.03	-0.04
C68	-0.04	-0.03	-0.04
C69	-0.04	-0.03	-0.04
C70	-0.27	-0.27	-0.27
C71	-0.27	-0.27	-0.27
C72	-0.27	-0.27	-0.27
C73	0.46	0.46	0.46
C74	0.46	0.46	0.46
C75	0.46	0.46	0.46
C76	-0.07	-0.07	-0.07
C77	-0.07	-0.07	-0.07
C78	-0.07	-0.07	-0.07

C79	0.06	0.06	0.06
C80	0.06	0.06	0.06
C81	0.06	0.06	0.06
C82	-0.04	-0.03	-0.04
C83	-0.04	-0.03	-0.04
C84	-0.04	-0.03	-0.04
N1	-0.27	-0.27	-0.27
N2	-0.27	-0.27	-0.27
N3	-0.27	-0.28	-0.27
N4	-0.27	-0.27	-0.27
N5	-0.27	-0.28	-0.27
N6	-0.27	-0.27	-0.27
N7	-0.58	-0.54	-0.12
N8	-0.58	-0.54	-0.12
N9	-0.58	-0.54	-0.12
N10	-0.58	-0.54	-0.12
N11	-0.58	-0.54	-0.13
N12	-0.58	-0.54	-0.12
S1	0.35	0.35	0.36
S2	0.35	0.35	0.36
S3	0.36	0.35	0.36
S4	0.35	0.35	0.36
S5	0.35	0.35	0.36
S6	0.35	0.35	0.36
O1		-	-0.09
O2		-	-0.09
O3		-	-0.09
S7	-	0.85	-
S8	-	0.85	-
S9	-	0.85	-
Se1	0.89	-	
Se2	0.89	-	
Se3	0.89	-	

Table S7. The free energy values of JUC-616, JUC-617 and JUC-618.

	JUC-616	**JUC-617**	**JUC-618**
ΔG_1	-0.4	-0.18	-0.37
ΔG_2	-0.54	-0.52	-0.17
ΔG_3	0.39	0.23	0.24
ΔG_4	0.55	0.47	0.3
Overpotential	0.55	0.52	0.37

3. References

1 S. Yang, X. Li, Y. Qin, Y. Cheng, W. Fan, X. Lang, L. Zheng and Q. Cao, *ACS Appl. Mater. Inter.*, 2021, **13**, 29471-29481.

2 J. Hafner, *J. Comput. Chem.*, 2008, **29**, 2044-2078.

3 Z. W. Seh, J. Kibsgaard, C. F. Dickens, I. Chorkendorff, J. K. Nørskov and T. F. Jaramillo, *Science*, 2017, **355**, eaad4998.

4 L. Vega, J. Ruvireta, F. Viñes and F. Illas, *J. Chem. Theory Comput.*, 2018, **14**, 395-403.

5 A. Dumi, S. Upadhyay, L. Bernasconi, H. Shin, A. Benali and K. D. Jordan, *J. Chem. Phys.*, 2022, **156**, 144702.

6 Y. Wang, P. Wisesa, A. Balasubramanian, S. Dwaraknath and T. Mueller, *Comput. Mater. Sci.*, 2021, **187**, 110100.

7 P. V. Laurikainen and E. L. Sarlin, *ACS Omega*, 2021, **6**, 29424-29431.

8 T. Lu and F. Chen, *J. Comput. Chem.*, 2012, **33**, 580-592.

9 G. Kresse and D. Joubert, *Phys. Rev. B.*, 1999, **59**, 1758-1775.

10 J. Perdew, K. Burke and M. Ernzerhof, *Phys. Rev. Lett.*, 1997, **78**, 3865-3868.

11 J. Greeley, I. E. L. Stephens, A. S. Bondarenko, T. P. Johansson, H. A. Hansen, T. F. Jaramillo, J. Rossmeisl, I. Chorkendorff and J. K. Nørskov, *Nat. Chem.*, 2009, **1**, 552-556.

12 J. Feng, S.-h. Luo, S.-x. Yan, Y. Zhan, Q. Wang, Y.-h. Zhang, X. Liu and L.-j. Chang, *Small*, 2021, **17**, 2101887.

13 Y. Wang, Y. Lv, Y. Su, L. Chen, H. Li and F. Wu, *Nano Energy*, 2021, **90**, 106589.

14 Z. Teng, W. Cai, W. Sim, Q. Zhang, C. Wang, C. Su and T. Ohno, *Appl. Catal. B Environ.*, 2021, **282**, 119589.

15 W. Hou and H. Xu, *J. Med. Chem.*, 2022, **65**, 4436-4456.

4. Author Contributions

Q. Fang, X. Liu, H. Li, S. Qiu, and V. Valtchev conceived the project, designed experiments and provided funding. J. Li conducted the experiments and analyzed the data. J. Jia, J. Suo, C. Li, Z. Wang provided experimental testing support and gave useful help during the experiments. X. Liu, J. Li and Q. Fang wrote the manuscript and discussed the results with all authors.